

The EUMETSAT Satellite Application Facility on Land Surface Analysis (LSA SAF)

Product User Manual Fire Detection and Monitoring (FD&M)

PRODUCT: LSA-29

The EUMETSAT
Network of
Satellite Application
Facilities




LSA SAF

Land Surface Analysis

Reference Number:
Issue/Revision Index:
Last Change:

SAF/LAND/IM/PUM_FD&M/1.0
Issue 1.0
15/03/2010


	PUM RFM	Doc: SAF/LAND/IM/PUM_FD&M/1.0 Issue: Version 1.0 Date: 15/03/2010
---	---------	---

DOCUMENT SIGNATURE TABLE

	Name	Date	Signature
Prepared by :	Malik Amraoui and Carlos C. DaCamara		
Approved by :	Land SAF Project Manager (IM)		

DOCUMENTATION CHANGE RECORD


Issue / Revision	Date	Description:
Version 1.0	15/03/2010	Version to be presented to ORR

	PUM RFM	Doc: SAF/LAND/IM/PUM_FD&M/1.0 Issue: Version 1.0 Date: 15/03/2010
---	---------	---

DISTRIBUTION LIST

Internal Consortium Distribution		
Organisation	Name	No. Copies
IM	Pedro Viterbo	
IM	Luís Pessanha	
IM	Isabel Trigo	
IDL	Carlos da Camara	
IM	Isabel Monteiro	
IM	Sandra Coelho	
IM	Carla Barroso	
IM	Pedro Diegues	
IM	Teresa Calado	
IM	Benvinda Barbosa	
IM	Ana Veloso	
IMK	Folke-S. Olesen	
IMK	Frank Goettsche	
IMK	Ewa Kabsch	
MF	Jean-Louis Roujean	
MF	Olivier Hauteceur	
MF	Dominique Carrer	
RMI	Françoise Meulenberghs	
RMI	Arboleda Alirio	
RMI	Nicolas Ghilain	
FMI	Niilo Siljamo	
UV	Joaquin Melia	
UV	F. Javier García Haro	
UV/EOLAB	Fernando Camacho	
UV	Alexander Verger	

External Distribution		
Organisation	Name	No. Copies
EUMETSAT	Frédéric Gasiglia	
EUMETSAT	Dominique Faucher	
EUMETSAT	Lorenzo Sarlo	
EUMETSAT	Lothar Schueller	
EDISOFT	Teresa Cardoso	
EDISOFT	Carlos Vicente	
EDISOFT	Cleber Balan	
SKYSOFT	Rui Alves	
SKYSOFT	João Canário	

	PUM RFM	Doc: SAF/LAND/IM/PUM_FD&M/1.0 Issue: Version 1.0 Date: 15/03/2010
---	---------	---

Steering Group Distribution		
Nominated by:	Name	No. Copies
IM	Carlos Direitinho Tavares	
EUMETSAT	Lorenzo Sarlo	
EUMETSAT	Yves Govaerts	
EUMETSAT	François Montagner	
STG/AFG (USAM)	Luigi de Leonibus	
MF	François Bouyssel	
RMI	Steven Dewitte	
FMI	Carl Fortelius	



	PUM RFM	Doc: SAF/LAND/IM/PUM_FD&M/1.0 Issue: Version 1.0 Date: 15/03/2010
---	---------	---

Table of Contents

DOCUMENT SIGNATURE TABLE	2
DOCUMENTATION CHANGE RECORD	2
1. Introduction.....	7
2. Algorithm.....	10
2.1. Overview	10
2.2. Objectives.....	12
3. Algorithm Description.....	12
3.1. Theoretical Description.....	12
3.1.1. Rationale.....	12
3.1.2. Mathematical Description of the Algorithm.....	13
3.2. Data description.....	19
3.2.1. Geolocation/Rectification.....	19
3.2.2. Input data	20
3.2.2.1. Static data	21
3.2.2.1. Dynamic data.....	21
3.2.3. Exception Handling.....	21
3.2.4. Output data.....	22
3.3. File Formats.....	26
3.4. Summary of Product Characteristics am.....	29
4. References	30
ANNEX A – Product Metadata – SEVIRI RFM.....	35


	<p>PUM RFM</p>	<p>Doc: SAF/LAND/IM/PUM_FD&M/1.0 Issue: Version 1.0 Date: 15/03/2010</p>
---	----------------	--

List of Tables

Table 1 LSA SAF products operational or under-development at the beginning of the 3 rd phase of the project – Continuous Development and Operations Phase (CDOP). Expected horizontal resolution and spatial coverage, generation frequency, and target accuracy are also indicated. Temporal resolution specifies the time interval to which the product applies.	8
Table 2 Product Requirements for FD&M, in terms of area coverage, resolution and accuracy.	10
Table 3. Maximum values for number of columns (ncol) and lines (nlin), for the Land-SAF geographical area of interest, and the respective COFF and LOFF coefficients needed to geolocate the data.	20
Table 4. SEVIRI channels used in FIDALGO.	21
Table 5 - Characteristics of geographical areas to process the algorithm.	22
Table 6 – Input data filters.	22
Table 7. Active fires and fire pixels over NAfr and SAfr windows during January and July 2007, respectively.	23
Table 8. Distribution of active fires among the different of GLC2000 land cover classes for NAfr and SAfr during January and July 2007, respectively.	24
Table 9. As in Table 4 but respecting to the EUR window during July-August 2008 and 2009.	25
Table 10 - Description of FD&M classification.	27
Table 11 - Names and description of dataset that composes the output metadata files of FD&M.	27
Table 12 - Description of variables in the datasets ELEM_HR, ELEM_SG and ELEM_NC.	28
Table 13 - Description of variables in the dataset ELEM_CF.	28

List of Figures

Figure 1 - The LSA SAF geographical areas.	9
Figure 2 Schematic overview of the processing stages of FIDALGO.	13
Figure 3 Mask of desert regions (grey pixels), inland water bodies (white pixels), urban zones (black pixels) and volcanoes (red pixels) over the African continent.	14
Figure 4 An example of fire pixels as identified over a selected region in the African continent using information from the Meteosat image obtained by SEVIRI at 23:00 UTC of 23/01/2007. a) map of Africa where the location of the region is indicated by the small rectangular frame; b) values (in K) of Tb(3.9) according to the colour bar on the left; c) values (in K) of $\Delta T = Tb(3.9) - Tb(10.8)$ according to the colour bar on the left; d) location of confirmed vegetation fires (pixels in black) by FIDALGO (see Step 4 of the algorithm).	15
Figure 5 Examples of contaminated pixels as identified in three selected regions in the African continent whose locations are given by the rectangular frames in the map of Africa (lower left panel). Images correspond to SEVIRI R(0.8) as obtained at 08:00 UTC of 23/01/2007 (A), 11:15 UTC of 22/01/2007 (B) and 17:15 UTC of 23/01/2007 (C). Pixels in cyan, in yellow and in red respectively indicate clouds, highly reflective surfaces and areas of sunglint.	17
Figure 6 Fire pixels over NAfr and SAfr windows, respectively during January and July 2007. The colour bar indicates for each fire pixel the number of identified active fires.	24
Figure 7 As in Figure 6 but respecting to active fires and fire pixels in the EUR window during July August 2008 (upper panel) and July-August 2009 (lower panel).	26

	<p>PUM RFM</p>	<p>Doc: SAF/LAND/IM/PUM_FD&M/1.0 Issue: Version 1.0 Date: 15/03/2010</p>
---	----------------	--

1. Introduction

LSA SAF is part of the SAF Network, i.e., specialised development and processing centres, which constitute EUMETSAT distributed Applications Ground Segment, along with the Central Facility in Darmstadt. The main purpose of the SAF dedicated to Land Surface Analysis is to take full advantage of remotely sensed data, particularly those available from EUMETSAT sensors, to describe/derive land surface properties/variables. The LSA SAF has started its 5-year development phase in September 1999, and its initial operations in January 2005 (DaCamara, 2006, Trigo et al., 2009).

User requirements evolve with the availability of improved/new data sources, and the rise of potential applications for new products. The design of Land-SAF products was initially driven by the needs of the meteorological, particularly NWP, community, considered the priority user for Land-SAF services. There is, however, a growing number of other important areas, including agricultural and forestry applications, land use, and the broader topics of climate and environment monitoring.

The involvement of the user community in the design of Land-SAF products, already established during the IOP, shall be a priority throughout its whole lifecycle. The targeted users include operational or research groups within

- (i) NWP community;
- (ii) agriculture and forest applications,
- (iii) food management,
- (iv) environment monitoring and risk assessment
- (v) hydrological applications
- (vi) climate modelling and monitoring
- (vii) other remote sensing applications

The LSA SAF has two operational chains dedicated to SEVIRI/Meteosat and AVHRR/MetOp processing, respectively. The Consortium also has a processing chain for validation and testing of new algorithm versions, before these are transferred to one of the operational suites. The LSA SAF operational system generates, archives and disseminates 8 pre-operational or demonstration products, based on SEVIRI data. AVHRR derived products are expected to become (pre-)operational during CDOP.

The spin-stabilised Meteosat Second Generation (MSG) has an imaging-repeat cycle of 15 minutes. The Spinning Enhanced Visible and Infrared Imager (SEVIRI) radiometer embarked on the MSG platform encompasses unique spectral characteristics and accuracy, with a 3 km resolution (sampling distance) at nadir (1km for the high-resolution visible channel), and 12 spectral channels (Schmetz et al., 2002).


	PUM RFM	Doc: SAF/LAND/IM/PUM_FD&M/1.0 Issue: Version 1.0 Date: 15/03/2010
---	---------	---

Table 1 LSA SAF products operational or under-development at the beginning of the 3rd phase of the project – Continuous Development and Operations Phase (CDOP). Expected horizontal resolution and spatial coverage, generation frequency, and target accuracy are also indicated. Temporal resolution specifies the time interval to which the product applies.


	Product	Horizontal Resolution & Coverage	Temporal Resolution	Generation Frequency	Target Accuracy
Surface Radiation Budget	AL – Albedo	MSG disk	5-day & 30-day	Daily & 10-day	10 %
	LST – Land Surface Temperature	MSG disk / Global*	Instantaneous	15min & 12-hourly*	2 K
	EM – Emissivity	MSG disk / Global*	5-day & 30-day	Daily & 10-day	5 %
	DSSF – Down-welling Surface Short-wave Flux	MSG disk / Global*	Instantaneous & Daily	30 min & Daily	5-10 %
	DSLFL – Down-welling Surface Long-wave Flux	MSG disk / Global*	Instantaneous & Daily	30 min & Daily	5-10 %
Biogeophysical Parameters I	SC – Snow Cover	MSG disk / Global	Daily	Daily	<3% false alarms >75% hit rate forest > 90% for other areas
	ET – Soil Moisture/ Evapotranspiration	MSG disk	Daily / 30 min	Daily / 30 min	20%
Biogeophysical Parameters II	FVC – Fraction of Vegetation Cover	MSG disk / Global*	5-day & 30-day	Daily & 10-day	10-15% (SEVIRI+AVHRR) 20% (SEVIRI)
	LAI – Leaf Area Index	MSG disk / Global*	5-day & 30-day	Daily & 10-day	25-30% (SEVIRI+AVHRR) 40% (SEVIRI)
	FAPAR – Fraction of Absorbed Photosynthetic Active Radiation	MSG disk / Global*	5-day & 30-day	Daily & 10-day	10-15% (SEVIRI+AVHRR) 20% (SEVIRI)
	RFM – Risk of Fire Mapping	Europe	Daily	Daily	Risk +/-2.5-5
	FD&M – Fire Detection & Monitoring	MSG disk	15-min & Daily	15-min & Daily	10-45%
	FRP – Fire Radiative Power	MSG disk	15-min & hourly	15-min & hourly	10-30%

*Global and 12-hourly products refer to retrievals from AVHRR/EPs.

**Indirectly, via other LSA SAF components (AL, DSSF, DSLFL, FVC, LAI, ...)

***For cloud identification and classification.

The EUMETSAT Polar System (EPS) is Europe's first polar orbiting operational meteorological satellite and the European contribution to a joint polar system with the U.S. EUMETSAT will have the operational responsibility for the "morning orbit" with

	PUM RFM	Doc: SAF/LAND/IM/PUM_FD&M/1.0 Issue: Version 1.0 Date: 15/03/2010
---	---------	---

Meteorological-Operational (MetOp) satellites, the first of which was successfully launched on October 19, 2006. Despite the wide range of sensors on-board MetOp (<http://www.eumetsat.int/>), most LSA SAF parameters make use of the Advanced Very High Resolution Radiometer (AVHRR) and, to a lesser extent, of the Advanced Scatterometer (ASCAT).

The LSA SAF products (Table 1) are based on level 1.5 SEVIRI/Meteosat and/or level 1b MetOp data. Forecasts provided by the European Centre for Medium-range Weather Forecasts (ECMWF) are also used as ancillary data for atmospheric correction.

The SEVIRI/Meteosat derived products are generated for 4 different geographical areas within Meteosat disk (Figure 1):

- Euro – Europe, covering all EUMETSAT member states;
- NAfr – Northern Africa encompassing the Sahara and Sahel regions, and part of equatorial Africa.
- SAfr – Southern Africa covering the African continent south of the Equator.
- SAmE – South American continent within the Meteosat disk.

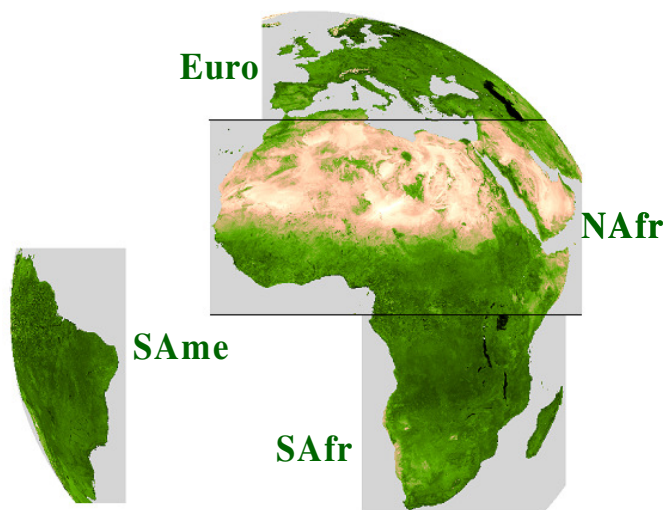



Figure 1 - The LSA SAF geographical areas.

MetOp derived parameters are currently available at level 1b full spatial resolution and for the processed Product Distribution Units (PDUs), each corresponding to about 3 minutes of instrument-specific observation data. Composite and re-projected products are foreseen for a later stage of the LSA SAF.

The LSA SAF system is fully centralized at IM and will be able to operationally generate, archive, and disseminate the operational products. The monitoring and quality control of the operational products, also centralized at IM, is performed automatically

	PUM RFM	Doc: SAF/LAND/IM/PUM_FD&M/1.0 Issue: Version 1.0 Date: 15/03/2010
---	---------	---

by the LSA SAF software, which provides quality information to be distributed with the products.

The LSA SAF products are currently available from LSA SAF website (<http://landsaf.meteo.pt>) that contains real time examples of the products as well as updated information.

This document is one of the product manuals dedicated to LSA SAF users. The algorithm and the main characteristics of the Fire Detection and Monitoring (FD&M) product generated by the LSA SAF from SEVIRI data system is described in the following sections. The characteristics of the SEVIRI-based FD&M product provided by the LSA SAF are described in Table 2. Further details on the LSA SAF product requirements may be found in the Product Requirements Document / Table (SAF_LAND_IM_PRT_1.7.XLS) available at the LSA SAF website <http://landsaf.meteo.pt>.

Table 2 Product Requirements for FD&M, in terms of area coverage, resolution and accuracy.


FD&M Product	Coverage	Resolution		Accuracy		
		Temporal	Spatial	Threshold	Target	Optimal
FD&M	MSG disk	15-min	MSG pixel resolution	100%	45%	10%

2. Algorithm

2.1. Overview

Fires are an important and highly variable source of air pollution emissions in many regions of the world and they constitute a significant, if not dominant, factor controlling the interannual variability of the atmospheric composition (Schultz et al., 2008). In this respect, African vegetation fires play a central role in tropical and subtropical atmospheric chemistry and, according to Lacaux et al. (1993), account for 57% of all tropical burning (49% from savanna fires and 8% from forest burns).


Estimates of global direct carbon emissions from wildland fires range from 1428 Tg C/year as estimated by Ito and Penner (2004) to 2771 Tg C/year as calculated by Galanter et al. (2000). According to the 41-year inventory of vegetation fire emissions constructed for the Reanalysis of the Tropospheric chemical composition over the past 40 years project (RETRO), the global total direct carbon emission flux from wildland fire emissions amounts to 2078 Tg C/year (Schultz et al., 2008), the African continent contributing to about one half of the global vegetation fire emissions; 24.75 % for northern Africa and 23.49 % for southern Africa. However, as pointed out by the authors, future versions of the inventory will benefit from ongoing analyses of burned areas based on satellite data.

	<p>PUM RFM</p>	<p>Doc: SAF/LAND/IM/PUM_FD&M/1.0 Issue: Version 1.0 Date: 15/03/2010</p>
---	----------------	--

Several studies have used remotely sensed data to characterize the seasonality of vegetation fires at the continental and global scales (Cahoon et al., 1992; Barbosa et al., 1999; Dwyer et al., 1999, 2000a,b; Schultz 2002; Generoso et al., 2003; Silva et al., 2003; Tansey et al., 2004a,b; Csiszar et al. 2005; Giglio et al., 2006; Le Page et al., 2008). All of these analyses relied on satellite systems with a frequency of overpass ranging from a minimum of every 3-4 days to a maximum of 4 times per day. In this respect it is worth mentioning the suite of the fire products derived from the Moderate Resolution Imaging Spectrometer (MODIS) sensor, both active fires and burnt area, which are made available by the Fire Information for Resource Management System (FIRMS) at the University of Maryland (USA). This is adequate to depict seasonal patterns extending over a period of a few months, but of limited utility to analyse higher frequency periodicities, such as daily, or even weekly fire cycles. In a recent work, Giglio (2007) characterized the average diurnal fire cycle in 15 regions of the tropics and subtropics using seven years of observations made with the Visible and Infrared Scanner (VIRS) and the MODIS instruments. The author noted that the diurnal cycle was prominent in all these regions, with a maximum of activity in the early-to late-afternoon and typically little or no burning between 00:00 and 08:00 local time.

Quantitative characterization of daily fire cycles is important for several reasons; i) the chemical composition of pyrogenic emissions is affected by dead fuel moisture content (Andreae and Merlet, 2001; Hoffer et al., 2006), which tracks the daily cycle of atmospheric relative humidity, with timelags that are a function of fuel particle size; ii) higher nocturnal atmospheric stability, and especially low-level inversions, may lead to decreased injection heights, thus restricting long-distance dispersal of combustion products (Garstang and Tyson, 1997); iii) the optical depth of biomass burning smoke aerosol displays a strong daily cycle (Smirnov et al., 2002; Eck et al., 2003) and generates radiative impacts that disturb cloud formation and convective rainfall patterns in the tropics (Rosenfeld, 1999; Smirnov et al., 2002; Andreae et al., 2004). Increasing the temporal resolution of vegetation fire data to hourly or even sub-hourly intervals may therefore contribute towards improving models of environmental processes affected by biomass burning. High frequency fire information is also relevant for civil protection and forest protection activities (Pereira and Govaerts, 2001).

Geostationary meteorological satellite systems provide much higher frequency of observation of the land surface than sun-synchronous systems but, until recently, their spatial and spectral resolutions were sub-optimal for vegetation fire monitoring. Nevertheless, various authors demonstrated the capability of earlier geostationary satellites to detect active fires (Prins and Menzel, 1992, 1994; Prins and Schmetz, 2000) and to estimate burned areas (Boschetti et al., 2003). New possibilities were opened up with the launch in 2002 of Meteosat-8, the first satellite of the Meteosat Second Generation (MSG). Temporal, spatial and spectral characteristics of the MSG series were substantially improved (Schmetz et al., 2002), rendering its satellites very adequate for Earth surface observation, and namely for fire monitoring (Cihlar et al., 1999; Pereira and Govaerts, 2001). The potential of MSG was promptly explored, namely by expanding the scope of previous fire applications of geostationary systems with the goal of quantifying fire intensity and biomass consumption (Roberts et al., 2005; Roberts and Wooster, 2008). In this respect the MPEF FIR product of EUMETSAT for thermal anomalies detection, currently disseminated via EUMETCast is also worth mentioning.

	PUM RFM	Doc: SAF/LAND/IM/PUM_FD&M/1.0 Issue: Version 1.0 Date: 15/03/2010
---	---------	---

The LSA SAF is currently exploring (i) the capability of SEVIRI/MSG to detect and monitor active fires, particularly over Africa and Europe, leading to the operational generation, archiving and dissemination of the so-called Fire Detection and Monitoring (FD&M) product; and (ii) combining meteorological information with characteristics of vegetation to produce meaningful danger of fire rating for Southern Europe. In this respect the hereafter described Risk of Fire Mapping (RFM) product may be viewed as representing the first attempt to make an integrated use of meteorological information from meteorological forecasts, vegetation data from land cover maps and observations of active fires and fire pixels as obtained from the RFM product of the LSA SAF in order to produce coherent maps of fire risk at the scale of MSG.

2.2. Objectives

The aim of FIDALGO is to identify, every 15 minutes, MSG pixels potentially contaminated with fires over the African and European continents.

Detection and systematic monitoring of active fires over the African continent is essential for an accurate assessment of the overall fire activity, namely in protected areas e.g. national parks, reserves and hunting concessions. It also allows characterising the fire regimes in African protected areas and more specifically assessing their impacts on the natural habitats and consequently on the biodiversity.

Active fire detection over Europe is in turn essential for early fire warning and for fire prevention, namely in what respects to a proper calibration of risk of fire indices, namely those that integrate the Risk of Fire Mapping (RFM) product currently being developed by the LSA SAF.


3. Algorithm Description

3.1. Theoretical Description

3.1.1. Rationale

Depending on whether they are smouldering or flaming, most fires burn at temperatures between 500 and 1200 K (Dwyer et al., 2000b) but even higher temperatures (>1400 K) may occur in forested areas (Giglio et al., 1999). At these temperatures and in accordance with Planck's theory of blackbody radiation, there is a very strong emission in the middle-infrared (MIR) at wavelengths of 3-5 μm , as opposed to the background where the peaks of emission are located in the long-wave infrared (IR) at wavelengths of the order of 10 μm .

Most of the existing operational fire detection algorithms were developed for regional, continental and global applications and have been tuned accordingly. Generally speaking, the techniques utilize similar processing steps and input data (predominantly short- and long-wave IR bands) and the algorithms may be placed in two broad categories: fixed-threshold techniques and spatial analysis (or contextual) techniques (Justice and Dowty, 1994). Earlier algorithms of fire detection relied on static

	<p>PUM RFM</p>	<p>Doc: SAF/LAND/IM/PUM_FD&M/1.0 Issue: Version 1.0 Date: 15/03/2010</p>
---	----------------	--

thresholds that were applied to the values recorded in MIR and IR channels. Appropriate values for the thresholds were computed empirically, depending on vegetation type, region and time of year.

More recent methods use contextual algorithms where values of thresholds are dynamically derived using appropriate statistics obtained from the neighbouring pixels. As pointed out by Flasse and Ceccato (1996), the main difference between contextual and fixed threshold algorithms is that a decision is made on a relative basis rather than on an absolute one; if the contrast between a given pixel and its surroundings is high enough then the pixel is identified as containing an active fire.

Contextual algorithms were first explored by Prins and Menzel (1992), using GOES data and by Justice et al. (1993) using AVHRR data. The approach was further adopted for global and regional fire monitoring (Eva and Flasse, 1996; Dwyer et al., 1998; Stroppiana et al., 2000), and for the World Fire Web initiative (Grégoire et al., 2000). More recently, the contextual approach was used by the MODIS Fire Team to develop a global daily active fire product using MODIS data (Justice et al., 2002; Giglio et al., 2003a). Details about the algorithm developed for SEVIRI are given in the next section which closely follows Amraoui et al. (2010).

3.1.2. Mathematical Description of the Algorithm

The FIDALGO algorithm builds upon the above-mentioned contextual algorithms for AVHRR and MODIS. As schematically shown in Figure 2, the method consists of the following four main steps; 1) Pre-processing, 2) Selection of potential fire pixels, 3) Detection of contaminated pixels and 4) Confirmation of active fire pixels.

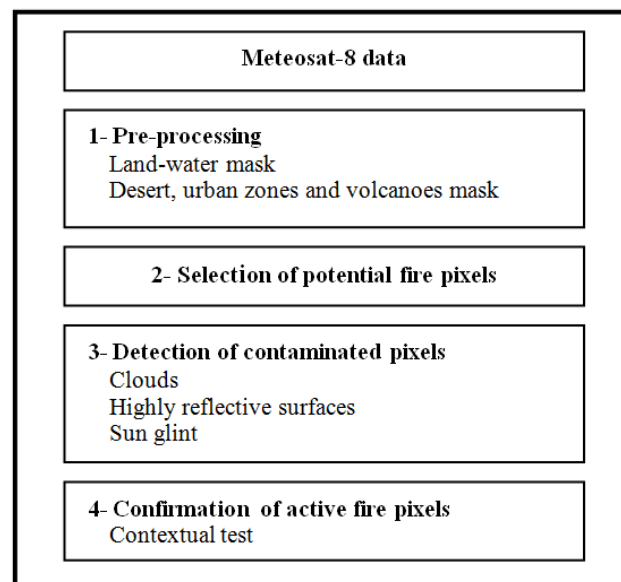



Figure 2 Schematic overview of the processing stages of FIDALGO.

	<p>PUM RFM</p>	<p>Doc: SAF/LAND/IM/PUM_FD&M/1.0 Issue: Version 1.0 Date: 15/03/2010</p>
---	----------------	--

Step 1 – Pre-processing

Surfaces such as exposed soil and rock are highly reflective at 3.9 μm , and may be the source of false fire detections. For instance, the algorithm by Arino et al. (1993) systematically identified large desert regions as very large burning areas, spanning thousands of pixels (Giglio et al., 1999; Mota et al., 2006).

A mask was accordingly defined that included pixels known to be associated with bare soils, inland water, volcanoes and urban zones. Land cover information from GLC2000 (Bartholomé and Belward, 2005) was used to generate a desert and water mask as well as to identify urban zones. Pixels contaminated by volcanoes were masked based on data from the Global Volcanism Program (<http://www.volcano.si.edu>). Figure 3 presents the defined mask over the African continent.

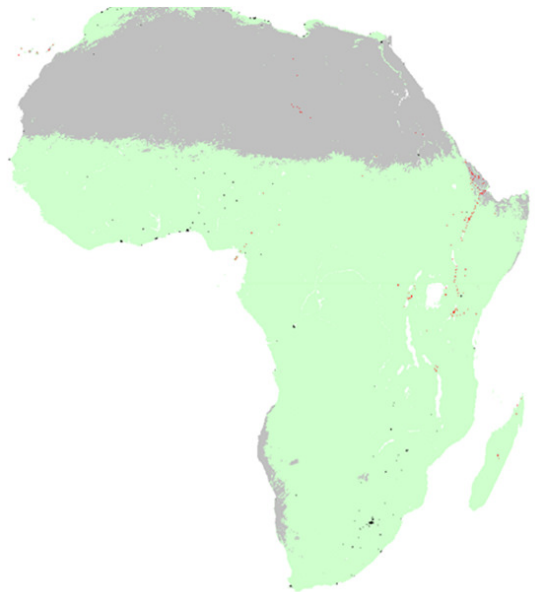



Figure 3 Mask of desert regions (grey pixels), inland water bodies (white pixels), urban zones (black pixels) and volcanoes (red pixels) over the African continent.

Step 2 – Selection of potential fire pixels

Selection of pixels likely to contain an active fire (Figure 4) may be achieved by simply applying, on a pixel-by-pixel basis, appropriate thresholds to MIR and to differences between MIR and IR channels (e.g., Arino et al., 1993; Flasse and Ceccato, 1996; Stroppiana et al., 2000; Justice et al., 2002; Giglio et al., 2003a,b).

Since the reflected MIR component increases with decreasing solar zenith angle, near solar noon a stronger reflected component may boost $Tb(3.9)$ above the prescribed threshold leading to the detection of spurious fires. On the other hand, as the solar

	<p>PUM RFM</p>	<p>Doc: SAF/LAND/IM/PUM_FD&M/1.0 Issue: Version 1.0 Date: 15/03/2010</p>
---	----------------	--

component drops off with increasing solar zenith angle, some small fires may not pass the threshold test (Giglio et al., 1999). With the aim of mitigating commission (omission) errors for low (high) solar zenith angles (SZA), during day time (i.e. for $SZA < 85^\circ$) thresholds imposed by FIDALGO both on $Tb(3.9)$ and on differences $\Delta T = Tb(3.9) - Tb(10.8)$ vary throughout the day. Accordingly, a pixel is considered as containing a potential fire if one of the following conditions is fulfilled:

$$\begin{aligned}
 & Tb(3.9) \geq 315K \text{ and } \Delta T \geq 10K \text{ for } SZA < 70^\circ \\
 & Tb(3.9) \geq 313K \text{ and } \Delta T \geq 9K \text{ for } 70^\circ \leq SZA < 73^\circ \\
 & Tb(3.9) \geq 311K \text{ and } \Delta T \geq 7K \text{ for } 73^\circ \leq SZA < 76^\circ \\
 & Tb(3.9) \geq 309K \text{ and } \Delta T \geq 5K \text{ for } 76^\circ \leq SZA < 79^\circ \\
 & Tb(3.9) \geq 307K \text{ and } \Delta T \geq 4K \text{ for } 79^\circ \leq SZA < 82^\circ \\
 & Tb(3.9) \geq 306K \text{ and } \Delta T \geq 3K \text{ for } 82^\circ \leq SZA < 85^\circ
 \end{aligned} \tag{1a}$$

During night time (i.e. for $SZA \geq 85^\circ$), a potential fire is attributed to a given pixel if the following condition holds:

$$Tb(3.9) \geq 305K \text{ and } \Delta T \geq 3K \text{ for } SZA \geq 85^\circ \tag{1b}$$

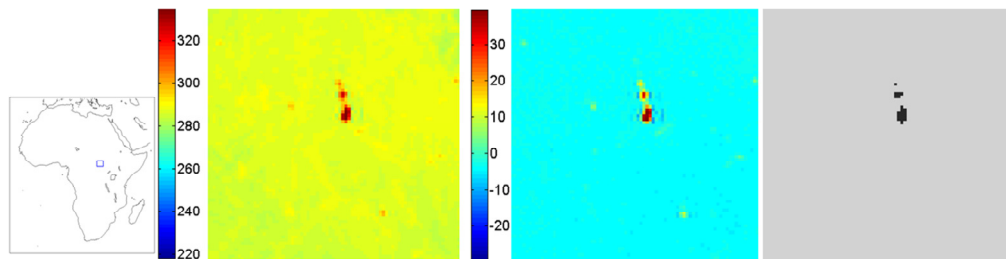



Figure 4 An example of fire pixels as identified over a selected region in the African continent using information from the Meteosat image obtained by SEVIRI at 23:00 UTC of 23/01/2007. a) map of Africa where the location of the region is indicated by the small rectangular frame; b) values (in K) of $Tb(3.9)$ according to the colour bar on the left; c) values (in K) of $\Delta T = Tb(3.9) - Tb(10.8)$ according to the colour bar on the left; d) location of confirmed vegetation fires (pixels in black) by FIDALGO (see Step 4 of the algorithm).

Step 3 – Detection of contaminated pixels

Contamination of channel $3.9 \mu m$ by clouds is the most commonly occurring source of false alarms during daytime. When illuminated by sunlight, clouds typically appear as regions of elevated $Tb(3.9)$ (due to reflected sunlight) and of reduced $Tb(10.8)$ (due to their cooler temperatures), leading to a net increase in ΔT that may give rise to an erroneous detection of pixels affected by active fires.

Several cloud identification techniques may be employed, ranging in quality from simple (e.g. spatially fixed thresholds) to highly sophisticated (inter-active analyst-controlled) ones. The following two extreme situations may result; (1) excessive cloud detection, which inadvertently masks fires, smoke and large cloud-free areas; (2) failure

	PUM RFM	Doc: SAF/LAND/IM/PUM_FD&M/1.0 Issue: Version 1.0 Date: 15/03/2010
---	---------	---

to mask most small and some large clouds, causing many false alarms (Giglio et al., 1999).

Cloud detection by FIDALGO is based on a simplified version of Saunders and Kriebel (1988) algorithm. A given day time pixel is considered as cloud or contaminated by clouds, and therefore eliminated, if one of the following three conditions is fulfilled, i.e.

$$R(0.6)+R(0.8)>1.2$$

or

$$Tb(12.0)<265K \quad (2a)$$

or

$$R(0.6)+R(0.8)>0.8 \text{ and } Tb(12.0)<285K$$

During night time, pixels are flagged as cloud if the following condition is satisfied:

$$Tb(12.0)<265K \quad (2b)$$

Since SEVIRI channel IR3.9 covers parts of both the solar and thermal ranges of the electromagnetic spectrum, it is crucial to reject those pixels whose values in the IR3.9 channel would be too high (or even saturate) due to high reflection, rather than high temperature (Flasse and Ceccato, 1996).

Accordingly, a given pixel is considered as representing a highly reflective surface and therefore eliminated if the following condition (Giglio et al., 1999) is fulfilled during daytime:

$$R(0.8)>0.25 \quad (3)$$

For certain sun-earth-satellite configurations false fire detections may occur due to specular reflexion of sunlight by water bodies, wet soils, cirrus clouds, cloud edges and, in rare instances, by bare soils (Stroppiana et al., 2000; Giglio et al., 2003a).

A given pixel is considered contaminated by sunglint, and therefore eliminated, if i) its neighbouring pixels are water bodies, sparsely vegetated or bare soils or contaminated by clouds and ii) the following condition is fulfilled during daytime:

$$SZA>40^\circ \text{ and } R(0.8)>0.20 \quad (4)$$

Examples of detection of contaminated pixels (clouds, highly reflective surfaces and areas of sunglint) are shown in Figure 5.

Step 4 – Confirmation of active fire pixels

A potential fire pixel is confirmed as a pixel containing an active fire by comparing its spectral signature against the radiative properties of the respective background (Kaufman et al., 1998). The background is defined as a 5×5 pixel grid centred at the potential fire pixel and valid background pixels are all those that i) were neither masked in step 3 nor identified as potential fire pixels in step 2 and ii) fulfill the following conditions:

$$\begin{aligned}
 &Tb(3.9) \geq 312K \text{ and } \Delta T \geq 10K \text{ for } SZA < 70^\circ \\
 &Tb(3.9) \geq 310K \text{ and } \Delta T \geq 9K \text{ for } 70^\circ \leq SZA < 73^\circ \\
 &Tb(3.9) \geq 308K \text{ and } \Delta T \geq 7K \text{ for } 73^\circ \leq SZA < 76^\circ \\
 &Tb(3.9) \geq 306K \text{ and } \Delta T \geq 5K \text{ for } 76^\circ \leq SZA < 79^\circ \\
 &Tb(3.9) \geq 304K \text{ and } \Delta T \geq 4K \text{ for } 79^\circ \leq SZA < 82^\circ \\
 &Tb(3.9) \geq 303K \text{ and } \Delta T \geq 3K \text{ for } 82^\circ \leq SZA < 85^\circ
 \end{aligned}
 \tag{5a}$$

during day time, or the following condition:

$$Tb(3.9) \geq 302K \text{ and } \Delta T \geq 3K \text{ for } SZA \geq 85^\circ
 \tag{5b}$$

during night time.

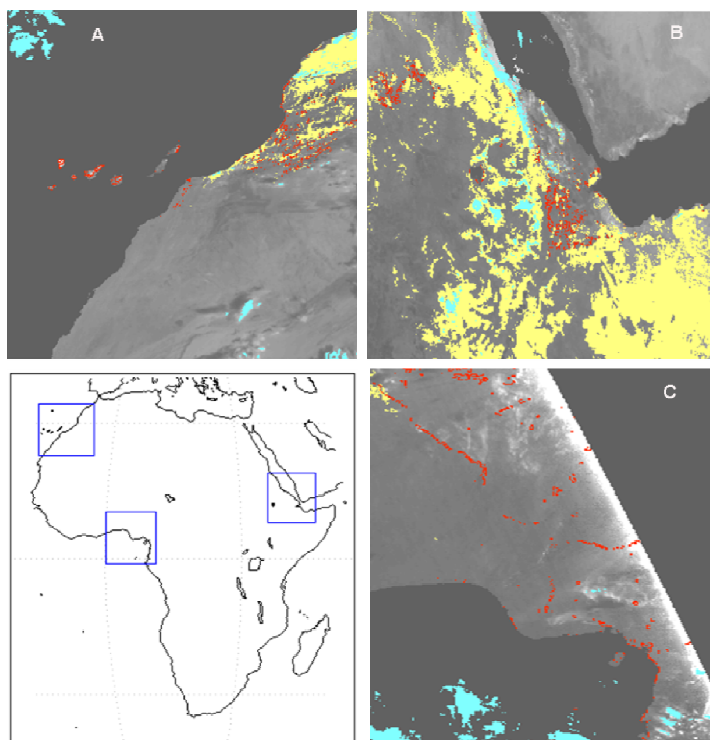


Figure 5 Examples of contaminated pixels as identified in three selected regions in the African continent whose locations are given by the rectangular frames in the map of Africa (lower left panel). Images correspond to SEVIRI R(0.8) as obtained at 08:00 UTC of 23/01/2007 (A), 11:15 UTC of 22/01/2007 (B) and 17:15 UTC of 23/01/2007 (C). Pixels in cyan, in yellow and in red respectively indicate clouds, highly reflective surfaces and areas of sunglint.

	PUM RFM	Doc: SAF/LAND/IM/PUM_FD&M/1.0 Issue: Version 1.0 Date: 15/03/2010
---	---------	---

Valid background pixels are then used to compute a set of statistics that characterise the background (Giglio et al., 1999), namely the mean and the absolute mean deviation of $Tb(3.9)$, respectively denoted as $\overline{Tb}(3.9)$ and $\delta(3.9)$:

$$\overline{Tb}(3.9) = \frac{1}{N} \sum_{i=1}^N Tb_i(3.9) \quad (6a)$$

$$\delta(3.9) = \frac{1}{N} \sum_{i=1}^N |Tb_i(3.9) - \overline{Tb}(3.9)| \quad (6b)$$

as well as the mean and absolute mean deviation of ΔT , respectively denoted as $\overline{\Delta T}$ and $\delta(\Delta T)$:

$$\overline{\Delta T} = \frac{1}{N} \sum_{i=1}^N \Delta T_i \quad (7a)$$

$$\delta(\Delta T) = \frac{1}{N} \sum_{i=1}^N |\Delta T_i - \overline{\Delta T}| \quad (7b)$$

The number of valid neighbouring pixels in the grid must be at least three, *i.e.* $N \geq 3$. If there is an insufficient number of valid surrounding pixels, statistics are not computed and the pixel is kept classified as potentially containing a fire.

A potential fire pixel is finally confirmed as a pixel containing an active fire when the two following conditions are met (Giglio et al., 1999):

$$Tb_{PF}(3.9) > \overline{Tb}(3.9) + \delta(3.9) - 3$$

and (8a)

$$\Delta T_{PF} > \overline{\Delta T} + \max(2.5 * \delta(\Delta T), 4)$$

during daytime, or the following condition:

$$\Delta T_{PF} > \overline{\Delta T} + \max(2.5 * \delta(\Delta T), 4) \quad (8b)$$

is fulfilled during night time. It may be noted that the subscript PF in the equations (8a) and (8b) indicates values corresponding to the potential fire pixel.

	PUM RFM	Doc: SAF/LAND/IM/PUM_FD&M/1.0 Issue: Version 1.0 Date: 15/03/2010
---	---------	---

3.2. Data description

3.2.1. Geolocation/Rectification

The **FD&M** SEVIRI-based fields are generated pixel-by-pixel, maintaining the original resolution of SEVIRI level 1.5 data. These correspond to rectified images to 0° longitude, which present a typical geo-reference uncertainty of about 1/3 of a pixel. Data are kept in the native geostationary projection.

Files containing the latitude and longitude of the centre of each pixel may be downloaded from the Land-SAF website (<http://landsaf.meteo.pt>; under “Static Data and Tools”):

Longitude

HDF5_LSASAF_MSG_LON_Euro_200512201600.bz2

Latitude

HDF5_LSASAF_MSG_LAT_Euro_200512201600.bz2

Alternatively, since the data are in the native geostationary projection, centred at 0° longitude and with a sampling distance of 3 km at the sub-satellite point, the latitude and longitude of any pixel may be easily estimated. Given the pixel column number, *ncol* (where *ncol*=1 correspond to the westernmost column of the file), and line number, *nlin* (where *nlin*=1 correspond to the northernmost line), the coordinates of the pixel may be estimated as follows:

$$lon = \arctg\left(\frac{s_2}{s_1}\right) + sub_lon \quad \text{longitude (deg) of pixel centre}$$

$$lat = \arctg\left(p_2 \cdot \frac{s_3}{s_{xy}}\right); \quad \text{latitude (deg) of pixel centre}$$

where

sub_lon is the sub-satellite point (*sub_lon*=0)

and

$$s_1 = p_1 - s_n \cdot \cos x \cdot \cos y$$

$$s_2 = s_n \cdot \sin x \cdot \cos y$$


$$s_3 = -s_n \cdot \sin y$$

$$s_{xy} = \sqrt{s_1^2 + s_2^2}$$

$$s_d = \sqrt{(p_1 \cdot \cos x \cdot \cos y)^2 - (\cos^2 y + p_2 \cdot \sin^2 y) \cdot p_3}$$

$$s_n = \frac{p_1 \cdot \cos x \cdot \cos y - s_d}{\cos^2 y + p_2 \cdot \sin^2 y}$$

where

	PUM RFM	Doc: SAF/LAND/IM/PUM_FD&M/1.0 Issue: Version 1.0 Date: 15/03/2010
---	---------	---

$$x = \frac{ncol - COFF}{2^{-16} \cdot CFAC} \quad (\text{in Degrees})$$

$$y = \frac{nlin - LOFF}{2^{-16} \cdot LFAC} \quad (\text{in Degrees})$$

$$p_1 = 42164$$

$$p_2 = 1.006803$$

$$p_3 = 1737121856$$

$$CFAC = 13642337$$

$$LFAC = 13642337$$

The CFAC and LFAC coefficients are column and line scaling factors which depend on the specific segmentation approach of the input SEVIRI data. Finally, COFF and LOFF are coefficients depending on the location of the each Land-SAF geographical area within the Meteosat disk. These are included in the file metadata (HDF5 attributes; Annex A), and correspond to the set of values detailed on Table 3 for SEVIRI/MSG areas of Europe, Northern Africa and Southern Africa.

Table 3. Maximum values for number of columns (ncol) and lines (nlin), for the Land-SAF geographical area of interest, and the respective COFF and LOFF coefficients needed to geo-locate the data.

Region Name	Description	Maximum <i>ncol</i>	Maximum <i>nlin</i>	COFF	LOFF
Euro	<u>Europe</u>	1701	651	308	1808
NAfr	<u>Northern Africa</u>	2211	1151	618	1158
SAfr	<u>Southern Africa</u>	1211	1191	-282	8

3.2.2. Input data

There are two kinds of input data required to properly run the algorithm:

- static data, which are delivered and updated by the developers of the FD&M algorithm;
- dynamic data, which are generated during the pre-processing phase at every time step.

3.2.2.1. Static data

One of the required static data is a file with the geographical location (longitude and latitude) of all volcanoes in a specific region (see Figure 4).

The other static data file is the GLC2000 land cover provided in the MSG projection for the specified regions in HDF5 format.

3.2.2.1. Dynamic data

As shown in Table 4, remotely-sensed information consists of top of the atmosphere (TOA) radiances of SEVIRI/Meteosat-8 at the maximal temporal resolution (i.e. every 15 minutes) for the following bands; visible channels centred at 0.635 μm (VIS0.6) and 0.81 μm (VIS0.8) and infrared channels centred at 3.92 μm (IR3.9), 10.8 μm (IR10.8) and 12.0 μm (IR12.0). TOA visible radiances from VIS0.6 and VIS0.8 were converted into reflectances, respectively referred to hereafter as R(0.6) and R(0.8). TOA infrared radiances from channels IR3.9, IR10.8 and IR12.0 were in turn converted into brightness temperatures, respectively denoted hereafter as Tb(3.9), Tb(10.8) and Tb(12.0). For each pixel and time-step, FIDALGO also makes use of the respective solar zenith angle.

Table 4. SEVIRI channels used in FIDALGO.

Channel	Purpose
R(0.6)	Cloud detection
R(0.8)	Cloud detection, bright surface and sunglint detection
Tb(3.9)	Active fire detection
Tb(10.8)	Active fire detection
Tb(12.0)	Cloud detection

3.2.3. Exception Handling

The algorithm may run in two modes of operation for a specific geographical region and date, the difference relying in the way channel IR039 is ingested in the algorithm ,i.e. either in the form of brightness temperature or in the for of channel radiance.

The geographical areas allowed by the algorithm are presented in Table 5. They are defined by the respective name and the corners position, relative to an MSG image of 3712 columns per 3712 lines, starting from North to South and from West to East.


	PUM RFM	Doc: SAF/LAND/IM/PUM_FD&M/1.0 Issue: Version 1.0 Date: 15/03/2010
---	---------	---

Table 5 - Characteristics of geographical areas to process the algorithm.

Region Name	Description	Initial Column	Final Column	Initial Line	Final Line	Size in Columns	Size in Lines	Total Number of Pixels
NAfr	<u>N</u> orthern <u>A</u> frica	1240	3450	700	1850	2211	1151	2.544.861
SAfr	<u>S</u> outhern <u>A</u> frica	2140	3350	1850	3040	1211	1191	1.442.301
Euro	<u>E</u> urope	463	2163	3013	3663	1701	651	1 107 351

When input values for a given pixel are not physically acceptable then a set of filters (Table 6) is applied to the input data to mask out all in this context. The filters are applied to the reflectances of channels VIS006 and VIS008 (Ref006 and Ref008) and to either the radiance or the brightness temperature of channel IR039 depending on the mode of operation.


Table 6 – Input data filters.

Variable	Condition	Assigned Value
Rad039	≤ 0	0.01
Tb039	< 0	-9999
Ref006	≥ 2	1
Ref006	< -1	-1
Ref008	≥ 2	1
Ref008	< -1	-1

3.2.4. Output data

The above-described procedure allows identifying both active fires (i.e. occurrences in a given pixel of a given image) and fire pixels (i.e. pixels where at least one active fire was detected). Identified fire pixels are further classified into the following three categories;

- Single occurrence fires defined as active fires that are isolated events in space and time, i.e. having occurred only once in the entire period and with no active fires identified in the neighbouring pixels neither in the same image nor in the previous and the following ones;
- Fires over sparse herbaceous or sparse shrub cover, defined as active fires occurring over pixels classified as belonging to GLC2000 class 14 (Table 1 and Figure 1);
- Vegetation fires which include all active fires that do not belong to the previous categories.

	PUM RFM	Doc: SAF/LAND/IM/PUM_FD&M/1.0 Issue: Version 1.0 Date: 15/03/2010
---	---------	---

As shown in Table 7, a grand total of 370 239 (325 923) active fires were detected, distributed over 73 046 (73 863) fire pixels within the NAfr (SAfr) window, during January (July) 2007. Single occurrences account for about 5% of active fires in both windows and fires over sparse herbaceous or sparse shrub cover represent about 2.5% in NAfr, being negligible in SAfr.

Table 7. Active fires and fire pixels over NAfr and SAfr windows during January and July 2007, respectively.

	NAfr	SAfr
Vegetation fires	341801	310771
Single occurrence	19581	15132
Sparse herb./shrub.	8857	20
Active fires	370239	325923
Fire pixels	73046	73863

Figure 6 presents the spatial distribution of identified active fires and fire pixels. Most burning activity over NAfr may be found in the Sahel region, especially in southern Chad, the Central African Republic, southern Sudan and in various regions of West Africa, with the exception of Nigeria, which displays lower fire density. Burning activity over SAfr is concentrated in northern Angola, the southern Democratic Republic of Congo and eastern Zambia.

Table 8 presents the distribution of vegetation fires among the different GLC2000 land cover classes. In both NAfr and SAfr windows, two classes clearly dominate: “Tree cover, broadleaved, deciduous, open”, containing 40 % of total fires observed, and “Shrub cover, closed-open, deciduous”, with 25 % of total fires in NAfr and 19 % in SAfr. It may be also noted that more than two-thirds (70%) of fires in SAfr were observed in GLC2000 classes dominated by trees (i.e. “Tree cover, broadleaved, evergreen”, “Tree cover, broadleaved, closed” and “Tree cover, broadleaved, deciduous, open”, in contrast with NAfr where the proportion is much lower (40%).

Ninety percent of NAfr fires concentrate in just four vegetation classes (bold, Table 8), namely “Tree cover, broadleaved, deciduous, open”, “Shrub cover, closed-open, deciduous”, “Mosaic: tree cover/other natural vegetation” and “Mosaic: cropland/shrub or grass cover”, respectively accounting for 40%, 25%, 17% and 8% of total fires. In SAfr, 93% of active fires also concentrate in four vegetation classes (bold, Table 8), namely “Tree cover, broadleaved, deciduous, open”, “Tree cover, broadleaved, closed”, “Shrub cover, closed-open, deciduous” and “Herbaceous cover, closed-open”, respectively accounting for 40%, 25%, 19% and 9% of total fires. There are two remarkable differences between the two hemispheres: whereas the “Tree cover, broadleaved, closed” class contains 25% of SAfr fires, this class is fire-free in NAfr. Conversely, the class “Mosaic: tree cover/other natural vegetation” encompasses 17% of all NAfr fires, but is unaffected in SAfr.

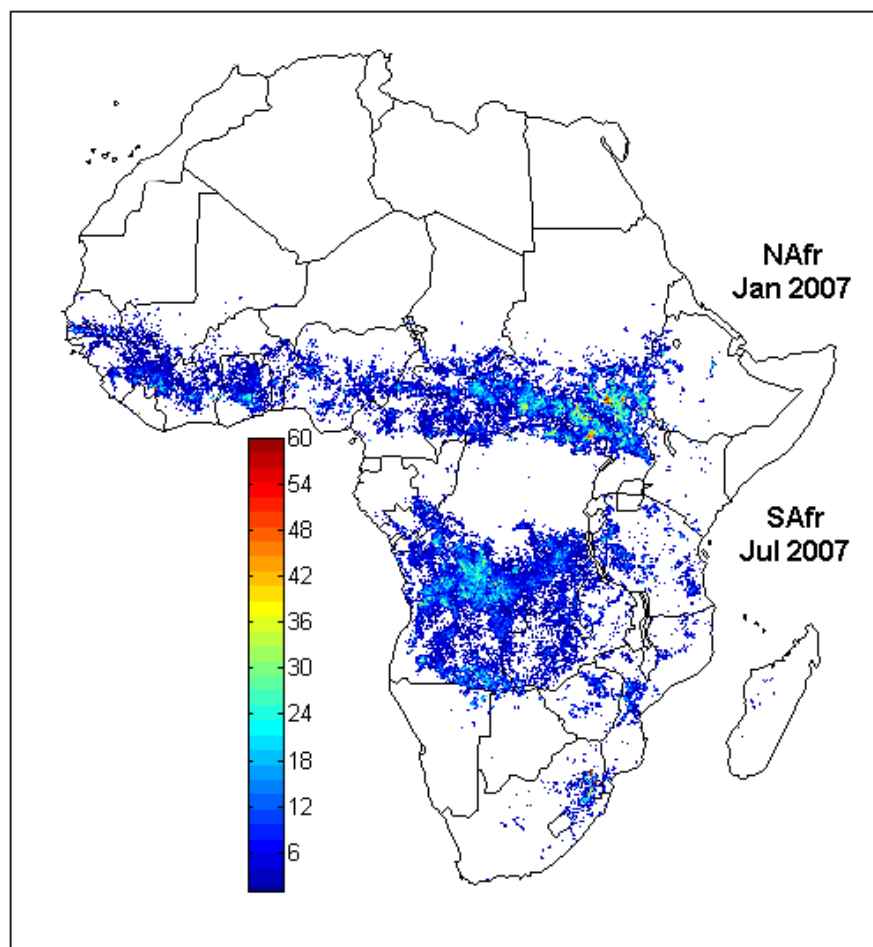



Figure 6 Fire pixels over NAfr and SAfr windows, respectively during January and July 2007. The colour bar indicates for each fire pixel the number of identified active fires.

Table 8. Distribution of active fires among the different of GLC2000 land cover classes for NAfr and SAfr during January and July 2007, respectively.

Code	Land cover type	NAfr (%)	SAfr (%)
1	Tree cover, broadleaved, evergreen	1	4
2	Tree cover, broadleaved, closed	0	25
3	Tree cover, broadleaved, deciduous, open	40	40
7	Tree cover, regularly flooded, fresh water	0	0
8	Tree cover, regularly flooded, saline water	0	0
9	Mosaic: tree cover/other natural vegetation	17	0
12	Shrub cover, closed-open, deciduous	25	19
13	Herbaceous cover, closed-open	3	9
15	Regularly flooded shrub and/or herbaceous cover	2	0
16	Cultivated and managed areas	1	3
17	Mosaic: cropland/tree cover/other natural vegetation	3	0
18	Mosaic: cropland/shrub or grass cover	8	0

	<p>PUM RFM</p>	<p>Doc: SAF/LAND/IM/PUM_FD&M/1.0 Issue: Version 1.0 Date: 15/03/2010</p>
---	----------------	--

It is worth pointing out that the observed fire incidence by land cover class compares well with the results of Barbosa et al. (1999) and Tansey et al. (2004a,b). The former authors used White's Vegetation of Africa map (White, 1983), and found that over 50% of the area burned, detected during the period 1982-1991, was located in three vegetation types, designated "Undifferentiated Ethiopian, Sudanian, and North Zambezian woodland", "Sudanian woodland with abundant Isoberlinia", and "Mosaic of Guineo-Congolian Lowland Forest and Secondary Grassland". An additional 20% of area burned affected "Wetter Zambezian Woodland Miombo", "Somalia-Masai Acacia-Commiphora Deciduous Bushland and Thicket", and "Drier Zambezian Miombo Woodland". Therefore, areas of open tree cover (*i.e.*, woodlands) are also found to be the vegetation type most affected by fire. Plate 3 of Barbosa et al. (1999) shows the location of the six most fire-prone African vegetation types, confirming the good match with our findings.

In their analysis of global area burned during the year 2000, Tansey et al. (2004a,b) identified the Northern Hemisphere sub-tropical shrubland and wooded grassland belt in Africa (with the exception of Somalia and Nigeria) as the region with the greatest burning activity per surface area in the world. In southern hemisphere Africa, peaks of burned area density were found in northern Angola and the southern Democratic Republic of Congo, also concurring with our own results.

Table 9 and Figure 7 provide information about fire activity during summer (defined as July + August) of 2008 and 2009. It is worth noting that, in 2009, although there are less fire pixels (3414) than in 2008 (3734) the larger duration observed (18866 in 2009 versus 11791 in 2008) provides an indication that summer 2009 was a more severe season in terms of fire duration and therefore in terms of burned area.

The spatial distribution of fire pixels and active fires clearly shows regions of high activity namely Portugal, Spain, southern France, Italy, Greece, Turkey, Croatia, Serbia, Romania, Bulgaria and Ukraine.

Table 9. As in Table 4 but respecting to the EUR window during July-August 2008 and 2009.

	Europe 2008	Europe 2009
Active fires	11791	18866
Fire pixels	3734	3414

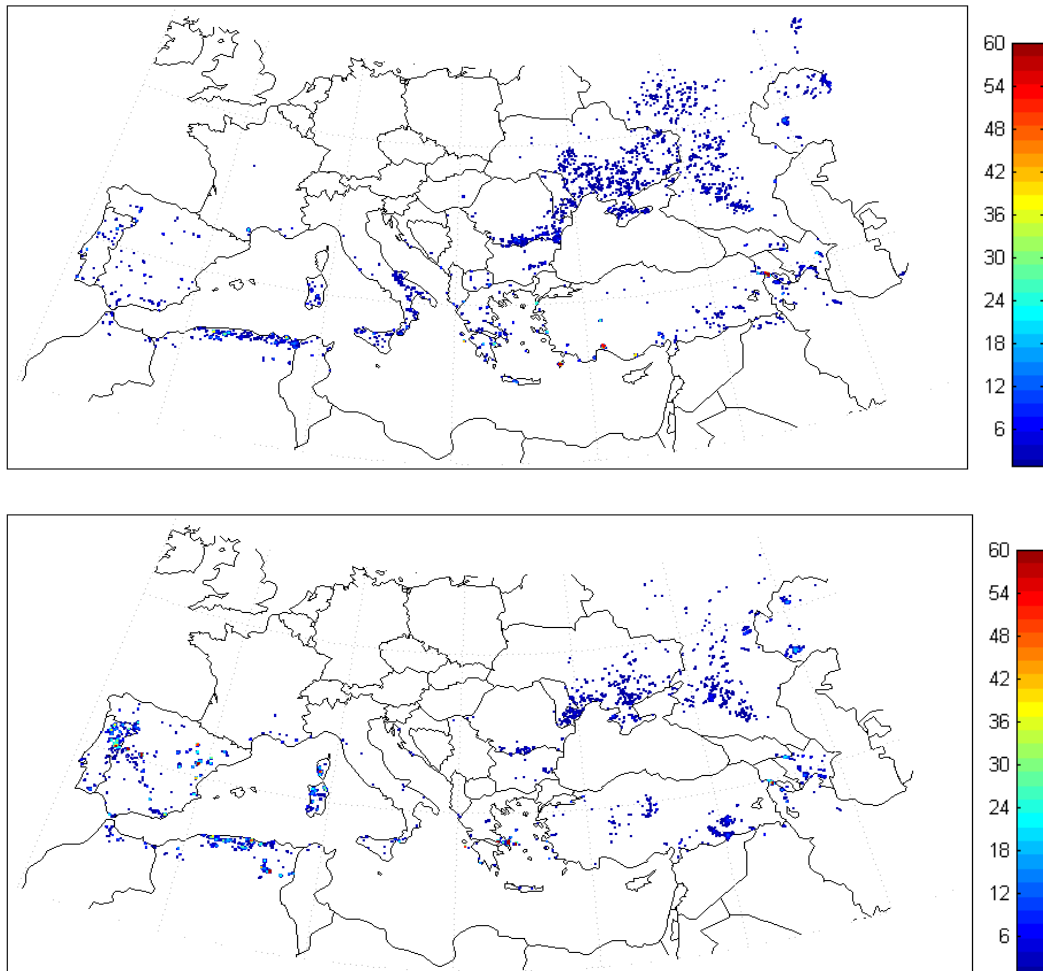


Figure 7 As in Figure 6 but respecting to active fires and fire pixels in the EUR window during July August 2008 (upper panel) and July-August 2009 (lower panel).

3.3. File Formats


At each time step the FD&M algorithm generates two external output files with: 1) FD&M classification and 2) the metadata, according to the following name convention:

1) **HDF5_LSASAF_MSG_FDeM_<Area>_YYYYMMDDHHMM**

and

2) **HDF5_LSASAF_MSG_FDeM-METADATA_<Area>_YYYYMMDDHHMM**

where <Area>, YYYY, MM, DD, HH and MM denote the geographical region (see **Error! Reference source not found.**), the year, the month, the day, the hour and the minute of data acquisition, respectively.

	PUM RFM	Doc: SAF/LAND/IM/PUM_FD&M/1.0 Issue: Version 1.0 Date: 15/03/2010
---	---------	---

FD&M product is provided in the HDF5 format as requested by the LSA-SAF system. This format allows defining a set of attributes that provide the relevant information. As described in **Error! Reference source not found.**, the main output file of FD&M product includes the general attributes (Table A), the dataset attributes (Table) and a raster dataset with the classification (Table 10) of each MSG pixel within a specific region (Table 5).

Table 10 - Description of FD&M classification.

# Class	Description
1	Water
2	Land
3	Land with fire

As described in the Annex A the RFM product information includes the general attributes (Table A 1) and the dataset attributes (Table A 2). Within the HDF5-files the information is organised in the form of separate datasets. An additional metadata file provides information about several relevant variables (Tables 11 and 12 for the pixels, if any, identified with i) sun glint, ii) high reflectivity, iii) confirmed and iv) not confirmed fires. This file includes one matrix dataset for each one of these items where columns correspond to the relevant variables and the lines correspond to the occurrence. The name of each dataset in the HDF5 file is pointed out in Table 11. If none of these items is detected, the output file is composed only by the general attributes and no datasets are included. The datasets ELEM_HR, ELEM_SG and ELEM_NC are only written if the “minimize_metadata” flag is turned OFF (=0).

Table 11 - Names and description of dataset that composes the output metadata files of FD&M.

Dataset Name	Description
ELEM_HR	Pixel <u>ELEM</u> ents identified with <u>H</u> igh <u>R</u> eflectivity
ELEM_SG	Pixel <u>ELEM</u> ents identified with <u>S</u> un <u>G</u> lint
ELEM_CF	Pixel <u>ELEM</u> ents with a <u>C</u> onfirmed <u>F</u> ire
ELEM_NC	Pixel <u>ELEM</u> ents with a <u>N</u> on <u>C</u> onfirmed Fire


	PUM RFM	Doc: SAF/LAND/IM/PUM_FD&M/1.0 Issue: Version 1.0 Date: 15/03/2010
---	---------	---

Table 12 - Description of variables in the datasets ELEM_HR, ELEM_SG and ELEM_NC.

# Column	Variable Description
1	Line of the pixel identified as high reflectivity, sun glint or non-confirmed fire
2	Column of the pixel identified as high reflectivity, sun glint or non-confirmed fire
3	Reflectivity of SEVIRI channel VIS006 [Adim.]
4	Reflectivity of SEVIRI channel VIS008 [Adim.]
5	Brightness temperature of SEVIRI channel IR039 [K]
6	Difference of brightness temperatures IR039 – IR108 [K]
7	Satellite zenith angle [°]
8	Brightness temperature of SEVIRI channel IR108 [K]
9	Brightness temperature of SEVIRI channel IR120 [K]

Table 13 - Description of variables in the dataset ELEM_CF.


# Column	Variable Description
1	Line of the pixel identified as a confirmed fire
2	Column of the pixel identified as a confirmed fire
5	Brightness temperature of SEVIRI channel IR039 [K]
6	Difference of brightness temperatures IR039 – IR108 [K]
7	Satellite zenith angle [°]
3	Reflectivity of SEVIRI channel VIS006 []
4	Reflectivity of SEVIRI channel VIS008 []
8	Brightness temperature of SEVIRI channel IR108 [K]
9	Brightness temperature of SEVIRI channel IR120 [K]

The algorithm also provides logging messages by using the **reportLog** (APID) [RD.2] function. The logging messages allow tracking the processing, which can help in debugging eventual errors. Each time step the RFM algorithm generates an external output file according to the following name convention:

HDF5_LSASAF_MSG_RFM_Euro_YYYYMMDDHHMM

where YYYY, MM, DD, HH and MM respectively, denote the year, the month, the day, the hour and the minute of data acquisition.

Libraries for handling HDF5-files in Fortran and C are available at <http://ftp.ncsa.uiuc.edu/HDF/HDF5/hdf5-1.6.2/>. A user friendly graphical interface to open and view HDF5-files may be downloaded from <http://hdf.ncsa.uiuc.edu/hdf-java-html/hdfview/>.

	PUM RFM	Doc: SAF/LAND/IM/PUM_FD&M/1.0 Issue: Version 1.0 Date: 15/03/2010
---	---------	---

3.4. Summary of Product Characteristics am

Product Name: Fire Detection and Monitoring
Product Code: FD&M
Product Level: Level 3
Description of Product: Fire Detection an Monitoring


Product Parameters:

Coverage: Euro, NAfr and SAfr
Packaging:
Units: Adimensional
Geo-location Requirements:
Format: 16 bits signed integer
Appended Data:
Frequency of generation: every 15-min
Size of Product:

Additional Information:


Identification of bands used in algorithm:
not applicable
Assumptions on SEVIRI input data:
not applicable
Identification of ancillary and auxiliary data:
2-m temperature (from ECMWF)
2-m dew point temperature (from ECMWF)
10-m zonal component of wind (from ECMWF)
10-m meridional component of wind (from ECMWF)
Cumulated precipitation in 24 h (from ECMWF)

The algorithm was coded following the rules specified in APID for Algorithm Integration and tested using a simulated **wrapper** as well as simulated **reportLog**, **stopping** and **getStopStatus** subroutines, all coded in FORTRAN 90. A Makefile is also provided to build the executable file. The product is prepared to run in stand-alone mode if all of the input data is available.

	PUM RFM	Doc: SAF/LAND/IM/PUM_FD&M/1.0 Issue: Version 1.0 Date: 15/03/2010
---	---------	---

4. References

- Amraoui, M., C.C. DaCamara, and J.M.C. Pereira (2010). Detection and monitoring of African vegetation fires using MSG-SEVIRI imagery. *Remote Sensing of Environment*, 114 (5), 1038-1052.
- Andreae, M.O. and P. Merlet. (2001). Emission of trace gases and aerosols from biomass burning. *Global Biogeochemical Cycles*, 15, 955-966, 2000GB001382.
- Andreae, M.O., D. Rosenfeld, P. Artaxo, A.A. Costa, G.P. Frank, K.M. Longo and M.A.F. Silva-Dias, (2004). Smoking rain clouds over the Amazon. *Science*, 303, 1337-1342.
- Arino, O., J.-M. Melinotte and G. Calabresi (1993). Fire, cloud, land, water: the “Ionia” AVHRR CD-Browser of ESRIN. EOQ 41, ESA, EST EC, Noordwijk, July 1993.
- Barbosa, P.M., D. Stroppiana, J.-M. Grégoire, and J.M.C. Pereira (1999). An assessment of vegetation fire in Africa (1981-1991): burned areas, burned biomass, and atmospheric emissions. *Global Biogeochemical Cycles* 13, 933-950.
- Bartholomé, E. and A.S. Belward (2005). GLC2000: A new approach to global land cover mapping from Earth observation data. *International Journal of Remote Sensing*, 26, 1959-1977.
- Boschetti, L., Brivio, P. A., and Gregoire, J. -M. (2003). The use of Meteosat and GMS imagery to detect burned areas in tropical environments. *Remote Sensing of Environment*, 85, 78-91.
- Cahoon, D.R., B.J. Stocks, J.S. Levine, W.R. Cofer and K.P. O'Neill (1992). Seasonal distribution of African savanna fires. *Nature*, 359, 812-815.
- Cihlar J., A. Belward and Y. Govaerts (1999). Meteosat Second Generation opportunities for land surface research and applications. EUMETSAT Scientific Publications EUM SP 01.
- Csiszar I., L. Denis, L. Giglio, C.O. Justice and J. Hewson (2005). Global fire activity from two years of MODIS data. *International Journal of Wildland Fire*, 14, 117-130, doi: 10.1071/WF03078.
- DaCamara C.C. (2006). The Land Surface Analysis SAF: one year of pre-operational activity. The 2006 EUMETSAT Meteorological Satellite Conference, Helsinki, Finland, 12-16 June 2006, EUMETSAT P.48, ISBN 92-9110-076-5, 8pp.
- Dwyer E., J.-M. Grégoire and J.P. Malingreau (1998). A global analysis of vegetation fires using satellite images: spatial and temporal dynamics. *Ambio*, 27, pp. 175-181.
- Dwyer, E., J.M.C. Pereira, J.-M. Grégoire and C.C. DaCamara (1999). Characterization of the spatio-temporal patterns of global fire activity using satellite imagery for the period April 1992 to March 1993, *Journal of Biogeography*, 27 (1), 57-69 (DOI: 10.1046/j.1365-2699.2000.00339.x).
- Dwyer E., J.-M. Grégoire and J.M.C. Pereira (2000a). Climate and vegetation as driving factors in global fire activity. In *Biomass burning and its inter-relationships with the climate*

	PUM RFM	Doc: SAF/LAND/IM/PUM_FD&M/1.0 Issue: Version 1.0 Date: 15/03/2010
---	---------	---

system, edited by J.L. Innes, M. Beniston and M.M. Verstraete, pp. 171-191, Springer, New York.

Dwyer E., S. Pincock, J.-M. Grégoire and J.M.C. Pereira (2000b). Global spatial and temporal distribution of vegetation fire as determined from satellite observations. *International Journal of Remote Sensing*, Vol. 21, No. 6, pp. 1289-1302.

Eck T.F., B.N. Holben, D.E. Ward, M.M. Mukelabai, O. Dubovik, A. Smirnov, J.S. Schafer, N.C. Hsu, S.J. Piketh, A. Queface, J. Le Roux, R.J. Swap and I. Slutsker (2003). Variability of biomass burning aerosol optical characteristics in Southern Africa during the SAFARI 2000 dry season campaign and a comparison of single scattering albedo estimates from radiometric measurements. *Journal of Geophysical Research*, Vol. 108, 8477, doi:10.1029/2002JD002321.

Eva H. and S. Flasse (1996). Contextual and multi-threshold algorithms for regional active fire detection with AVHRR data. *Remote Sensing Reviews*, Vol. 14, pp. 333-351.

Flasse S.P. and P. Ceccato (1996). A contextual algorithm for AVHRR fire detection. *International Journal of Remote Sensing*, Vol. 17, No. 2, pp. 419-424.

Galanter M., H. Levy II and G.R. Carmichael (2000). Impacts of biomass burning on tropospheric CO, NO_x and O₃. *Journal of Geophysical Research*, Vol. 105, pp. 6633-6653.

Garstang M. and P.D. Tyson (1997). Atmospheric circulation, vertical structure and transport over Southern Africa during the SAFARI-92 campaign. In *Fire in Southern Africa Savannas: Ecological and Atmospheric Perspectives* (B.W. van Wilgen, M.O. Andreae, J.G. Goldammer and J.A. Lindesay, Eds.), pp. 57-88. Witwatersrand University Press, Johannesburg, South Africa.


Generoso S., F.-M. Balkanski, O. Boucher and M. Schulz (2003). Improving the seasonal cycle and interannual variations of biomass burning aerosol sources. *Atmos. Chem. Phys.*, 3, pp. 1211-1222.

Giglio L., J.D. Kendall and C.O. Justice (1999). Evaluation of global fire detection algorithms using simulated AVHRR infrared data. *International Journal of Remote Sensing*, Vol. 20, No. 10, pp. 1947-1985.


Giglio L., J. Descloitres, C.O. Justice and Y.J. Kaufman (2003a). An enhanced contextual fire detection algorithm for MODIS. *Remote Sensing of Environment*, Vol. 87, pp. 273-282.

Giglio L., D. Kendall and R. Mack (2003b). A multi-year active fire dataset for the tropics derived from the TRMM VIRS. *International Journal of Remote Sensing*, Vol. 24, No. 22, pp. 4505-4525.


Giglio L., I. Csizsar and C.O. Justice (2006). Global distribution and seasonality of active fires as observed with the Terra and Aqua Moderate Resolution Imaging Spectroradiometer (MODIS) sensors. *Journal of Geophysical Research*, Vol. 111, G02016, doi:10.1029/2005JG000142.

	PUM RFM	Doc: SAF/LAND/IM/PUM_FD&M/1.0 Issue: Version 1.0 Date: 15/03/2010
---	---------	---


- Giglio L. (2007). Characterization of the tropical diurnal fire cycle using VIRS and MODIS observations. *Remote Sensing of Environment*, Vol. 108(4), pp. 407-421.
- Grégoire J.-M., D.R. Cahoon, D. Stroppiana, S. Pinnock, H. Eva, O. Arino, J.M. Rosaz and I. Csizsar (2000). Forest fire monitoring and mapping for GOF: current products and information networks based on NOAA-AVHRR, ERS-ATSR and SPOT-VGT systems. *Forest Fire Monitoring and Mapping: A component of Global Observation of Forest Cover*. Italy: Joint Research Centre, Ispra, pp. 111-135.
- Hoffer A., A. Gelencsér, M. Blazsó, P. Guyon, P. Artaxo and M.O. Andreae (2006). Diel and seasonal variations in the chemical composition of biomass burning aerosol. *Atmos. Chem. Phys.*, 6, pp. 3505-3515.
- Ito, A. and J.E. Penner (2004). Global estimates of biomass burning emissions based on satellite imagery for the year 2000. *Journal of Geophysical Research*, Vol. 109, D14S05, doi:10.1029/2003JD004423
- Justice C.O., J.P. Malingreau and A.W. Setzer (1993). Satellite remote sensing of fires: potential and limitations. *Fire in the Environment: the Ecological Atmospheric, and Climatic Importance of Vegetation Fires*, edited by P.J. Crutzen and J.G. Goldammer (New York: J. Wiley and Sons), pp. 77-88.
- Justice C.O. and P. Dowty (1994). IGBP-DIS satellite fire detection algorithm workshop technical report. *IGBP-DIS Working Paper 9*, NASA/GSFC, Greenbelt; Maryland; USA.
- Justice C.O. and J.P. Malingreau (editors) (1996). The IGBP-DIS fire algorithm workshop 2. IGBP-DIS Working Paper 14, Ispra Italy, October 1995.
- Justice C.O., L. Giglio, S. Korontzi, J. Owens, J.T. Morissette, D. Roy, J. Descloitres, S. Alleaume, F. Petitcolin and Y. Kaufman (2002). The MODIS fire products. *Remote Sensing of Environment*, Vol. 83, pp. 244-262.
- Kaufman, Y. L., Justice, C. O., Flynn, L., Kendall, J. D., Prins, E., Giglio, L., et al. (1998). Potential global fire monitoring from EOS-MODIS. *Journal of Geophysical Research*, 103, 215–238.
- Lacaux J.-P., H. Cachier and R. Delmas (1993). Biomass burning in Africa: an overview of its impact on atmospheric chemistry. In: *Fire in the Environment: The Ecological, Atmospheric, and Climatic Importance of Vegetation Fires*. Ed. P.J. Crutzen and J.G. Goldammer, J.Wiley and Sons, Chichester, UK.
- Le Page, Y., J.M.C. Pereira, R.M. Trigo, C.C. DaCamara, D. Oom and B. Mota (2008). Global fire activity patterns (1996-2006) and climatic influence: an analysis using the World Fire Atlas, *Atmos. Chem. Phys.*, 8, 1911-1924.
- Mota B., J.M.C. Pereira, D. Oom, M.J.P. Vasconcelos and M. Schultz (2006). Screening the ESA ATSR-2 World Fire Atlas (1997-2002). *Atmospheric Chemistry and Physics*, Vol. 6: 1409-1424.
- Pereira J.M.C. and Y. Govaerts (2001). Potential fire applications from MSG/SEVIRI observations. EUMETSAT Programme Development Department, Technical Memorandum No. 7.

	PUM RFM	Doc: SAF/LAND/IM/PUM_FD&M/1.0 Issue: Version 1.0 Date: 15/03/2010
---	---------	---

- Prins E.M. and W.P. Menzel (1992). Geostationary satellite detection of biomass burning in Southern America. *International Journal of Remote Sensing*, Vol. 13, pp. 2783-2799.
- Prins E.M. and W.P. Menzel (1994). Trends in South American biomass burning detected with the GOES VAS from 1983-1991. *Journal of Geophysical Research*, 99 (D8), pp. 16719-16735.
- Prins E.M., and J. Schmetz (2000). Diurnal active fire detection using a suite of international geostationary satellites. In *Forest Fire Monitoring and Mapping: A Component of Global Observation of Forest Cover*, (F. Ahern, J.-M. Grégoire and C. Justice, eds.), pp.139-148. European Commission Joint Research Centre, EUR19588EN.
- Roberts G., M.J. Wooster, G.L.W. Perry, N. Drake, L-M. Rebelo and F. Dipotso (2005). Retrieval of biomass combustion rates and totals from fire radiative power observations: application to southern Africa using geostationary SEVIRI Imagery. *Journal of Geophysical Research* 110, D21111: doi: 10.1029/2005JD006018.
- Roberts G.J. and M.J. Wooster (2008). Fire detection and fire characterization over Africa using Meteosat SEVIRI. *IEEE Transactions on Geoscience and Remote Sensing*, Vol. 46, No. 4, pp. 1200-1218.
- Rosenfeld, D. (1999). TRMM observed first direct evidence of smoke from forest fires inhibiting rainfall. *Geophysical Research Letters*, 26 (20), pp. 3105-3108.
- Saunders R.W. and K.T. Kriebel (1988). An improved method for detecting clear sky and cloud radiances from AVHRR data. *International Journal of Remote Sensing*, Vol. 9, pp. 123-150.
- Schmetz J., P. Pili, S. Tjemkes, D. Just, J. Kerkmann, S. Rota and A. Ratier (2002). An introduction to Meteosat Second Generation (MSG), Bulletin of the American Meteorological Society 83 (7), pp. 977-992 doi:10.1175/1520-0477(2002)083
- Schultz M.G. (2002). On the use of ATSR fire count data to estimate the seasonal and interannual variability of vegetation fire emissions. *Atmos. Chem. Phys.*, 2, pp. 387-395.
- Schultz, M.G., A. Heil, J.J. Hoelzemann, A. Spessa, K. Thonicke, J.G. Goldammer, A.C. Held, J.M.C. Pereira, and M. van het Bolscher (2008). Global wildland fire emissions from 1960 to 2000. *Global Biogeochemical Cycles*, Vol. 22, GB2002, doi:10.1029/2007GB003031
- Silva J.M.N., J.M.C. Pereira, A.I. Cabral, A.C.L. Sá, M.J.P. Vasconcelos, B. Mota and J.-M. Grégoire (2003). An estimate of area burned in Southern Africa during the 2000 dry season using SPOT-VEGETATION satellite data. *Journal of Geophysical Research*, Vol. 108, 8498, doi:10.1029/2002JD002320.
- Smirnov A., B.N. Holben, T.F. Eck, I. Slutsker, B. Chatenet and R.T. Pinker (2002). Diurnal variability of aerosol optical depth observed at AERONET (Aerosol Robotic Network) sites. *Geophysical Research Letters*, 29 (23), 2115, doi:10.1029/2002GL016305.

	<p>PUM RFM</p>	<p>Doc: SAF/LAND/IM/PUM_FD&M/1.0 Issue: Version 1.0 Date: 15/03/2010</p>
---	----------------	--

- Stroppiana D., S. Pinnock and J.-M. Grégoire (2000). The global fire product: daily fire occurrence from April 1992 to December 1993 derived from NOAA AVHRR data. *International Journal of Remote Sensing*, Vol. 21, No. 6, pp. 1279-1288.
- Tansey K.J., J.-M. Grégoire, D. Stroppiana, A. Sousa, J. Silva, J.M.C. Pereira, L. Boschetti, M. Maggi, P. Brivio, R. Fraser, S. Flasse, D. Ershov, E. Binaghi, D. Graetz and P. Peduzzi (2004a). Vegetation burning in the year 2000: global burned area estimates from SPOT VEGETATION data. *Journal of Geophysical Research*, doi:10.1029/2003JD003598.
- Tansey, K., J.-M. Grégoire, E. Binaghi, L. Boschetti, P.A. Brivio, D. Ershov, S. Flasse, R. Fraser, D. Graetz, M. Maggi, P. Peduzzi, J.M.C. Pereira, J. Silva, A. Sousa e D. Stroppiana (2004b). A global inventory of burned areas at 1 km resolution for the year 2000 derived from SPOT VEGETATION data. *Climatic Change* 67: 345–377.
- Trigo I., DaCamara, C., Viterbo, P., Roujean, J.L., Olesen, F., Barroso, C., Camacho-de Coca, F., Carrer, D., Freitas, S., García-Haro, F., Geiger, B., Gellens-Meulenberghs, F., Meliá, J., Ghilain, N., Pessanha, L., Siljamo, N. and Arboleda, A., 2009: The Satellite Application Facility on Land Surface Analysis. *Int. J. Rem Sens.* (in press).
- White, F. (1983). The vegetation of Africa, a descriptive memoir to accompany the UNESCO/AETFAT/UNSO vegetation map of Africa. UNESCO, Natural resources research, XX, 356 pp.


	<p>PUM RFM</p>	<p>Doc: SAF/LAND/IM/PUM_FD&M/1.0 Issue: Version 1.0 Date: 15/03/2010</p>
---	----------------	--

ANNEX A – Product Metadata – SEVIRI RFM

Table A 1 General attributes of the files for the SEVIRI FD&M product.

Attribute	Data Type	Values
SAF	String<3>	LSA
CENTRE	String<5>	IM-PT
ARCHIVE_FACILITY	String<5>	IM-PT
PRODUCT	String<79>	FD&M (main output file) FD&M-METADATA (metadata file)
PARENT_PRODUCT_NAME	Array(4) of string<79>	-
SPECTRAL_CHANNEL_ID	Int	1558 Channels VIS006, VIS008, IR039, IR108, and IR120
PRODUCT_ALGORITHM_VERSION	String<4>	2.00
CLOUD_COVERAGE	String<20>	-
OVERALL_QUALITY_FLAG	String<3>	OK
ASSOCIATED_QUALITY_INFORMATION	String<511>	-
REGION_NAME	String<4>	One of: NAfr or SAfr
COMPRESSION	Int	0
FIELD_TYPE	String<255>	Product
FORECAST_STEP	Int	0
NC	Int	Depend on REGION_NAME
NL	Int	Depend on REGION_NAME
NB_PARAMETERS	Int	1 (main output file) 0 to 4 (metadata file)
NOMINAL_PRODUCT_TIME	String<14>	YYYYMMDDhhmmss
SATELLITE	Array[10] of String<9>	{MSG}* [*]
INSTRUMENT_ID	Array [10] of String<6>	SEVI
INSTRUMENT_MODE	String<511>	STATIC_VIEW
IMAGE_ACQUISITION_TIME	String<14>	YYYYMMDDhhmmss
ORBIT_TYPE	String<3>	GEO

* {MSG}='MSG1', 'MSG2', 'MSG3',...

	<p>PUM RFM</p>	<p>Doc: SAF/LAND/IM/PUM_FD&M/1.0 Issue: Version 1.0 Date: 15/03/2010</p>
---	----------------	--

Attribute	Data Type	Values
PROJECTION_NAME	String<15>	Geos<0.0>
NOMINAL_LONG	Real	Read from SZA input file
NOMINAL_LAT	Real	Read from SZA input file
CFAC	Int	Read from SZA input file
LFAC	Int	Read from SZA input file
COFF	Int	Read from SZA input file
LOFF	Int	Read from SZA input file
START_ORBIT_NUMBER	Int	0
END_ORBIT_NUMBER	Int	0
SUB_SATELLITE_POINT_START_LAT	Real	0
SUB_SATELLITE_POINT_START_LON	Real	0
SUB_SATELLITE_POINT_END_LAT	Real	0
SUB_SATELLITE_POINT_END_LON	Real	0
SENSING_START_TIME	String<14>	YYYYMMDDhhmmss
SENSING_END_TIME	String<14>	YYYYMMDDhhmmss
PIXEL_SIZE	String<10>	3.1km
GRANULE_TYPE	String<2>	DP
PROCESSING_LEVEL	String<2>	03
PRODUCT_TYPE	String<8>	LSAFDeM
PRODUCT_ACTUAL_SIZE	Integer > 0, encoded as String<11>	Depends on number of bytes per pixel and on region
PROCESSING_MODE	String<1>	N
DISPOSITION_FLAG	String<1>	O
TIME_RANGE	String<20>	15-min
STATISTIC_TYPE	String<20>	-
MEAN_SSLAT	Real	Read from SZA input file
MEAN_SSLON	Real	Read from SZA input file
PLANNED_CHAN_PROCESSING	Integer	2
FIRST_LAT		0
FIRST_LON		0


	<p>PUM RFM</p>	<p>Doc: SAF/LAND/IM/PUM_FD&M/1.0 Issue: Version 1.0 Date: 15/03/2010</p>
---	----------------	--

Table A 2 Attributes of the FD&M/SEVIRI dataset.

Attribute	Data Type	Value
CLASS	String	Data
PRODUCT	String	CF (main output file) ELEM_HR, ELEM_SG, ELEM_CF or ELEM_NC 8 (metadata file)
PRODUCT_ID	Int	255
N_ COLS	Int	Depend on REGION_NAME
N_ LINES	Int	Depend on REGION_NAME
NB_BYTES	Int	2 (main output file) 8 (metadata file)
SCALING_FACTOR	Real	1
OFFSET	Real	0
MISSING_VALUE	Int	-1
UNITS	String	-
CAL_SLOPE	Real	0
CAL_OFFSET	Real	0